A REVIEW OF AERONAUTICAL FATIGUE AND STRUCTURAL INTEGRITY IN ISRAEL
(2021 –2023)

Compiled by:
Dr. Yuval Freed
Engineering Division
Israel Aerospace Industries
***Ben-Gurion Airport*, Israel**
yfreed@iai.co.il

A REVIEW OF AERONAUTICAL FATIGUE AND STRUCTURAL INTEGRITY IN ISRAEL

JANUARY 2021 – DECEMBER 2022

SUMMARY

This review summarizes fatigue, structural-integrity and fracture-mechanics investigations that were performed in Israel during the period of January 2021 to December 2022. The review includes contributions from Israel Aerospace Industries Ltd. (IAI), Tel-Aviv University (TAU), Ben-Gurion University (BGU), Ariel University (ARIEL) and Israel Airforce (IAF).

TABLE OF CONTENTS

A REVIEW OF AERONAUTICAL FATIGUE INVESTIGATIONS IN ISRAEL JANUARY 2017 – DECEMBER 2018

1. INTRODUCTION

The Israel National Review summarizes activities performed in the field of aeronautical fatigue, structural integrity, health monitoring and fracture mechanics in Israel during the period of January 2021 to December 2022. The previous National Review [1] covered activities up to the end of 2020. The following organizations contributed to this review:

- Israel Aerospace Industries Ltd. (IAI)
- Tel-Aviv University (TAU)
- Israel Airforce (IAF)
- Ben-Gurion University (BGU)
- Ariel University (ARIEL)

The National Review was compiled by Dr. Yuval Freed (yfreed@iai.co.il).

2. STRUCTURAL INTEGRITY OF METALLIC STRUCTURES

2.1 Aircraft loads assessment and its effect on aircraft structure - machine learning approach (Y. Freed, IAI)

The development of modern air-vehicles is a harmonized activity of numerous disciplines, such as aerodynamic sciences, propulsion, materials science, structural analysis, systems, avionics, manufacturing and more. The airframe design is based on data provided from these disciplines (for example, updated loads, weight, mass distributions and more). These data are usually provided to the designer in predetermined milestones that are correlated to logistic considerations (such as manufacturing preparations or purchasing of long lead items), all in light of the expected entry to market date.

In today competitive market of commercial aircraft, the entry to market date is extremely important. To meet such an aggressive deadline, the design drawings may be released prior to completion of structural substantiation for the most updated external loads. If the mature loads loops are issued relatively late in the development phase, there is a great risk that retrofits in structural parts that were already manufactured will be required. Such retrofits impact the program schedule and costs. To overcome this difficulty, it is highly important that the stress engineer will be able to assess the external loads loops upon their issuance, so unnecessary retrofits or redesigns of structural parts can be prevented.

The structural substantiation process is described in Figure 1. The failure criteria are chosen with respect to a given structural detail, and the margin of safety is obtained as the ratio $F_{all}/F_{app} - 1$, with F_{all} and F_{app} are the allowed and applied loads, respectively. In large scale development programs with thousands of external load cases, revised stress analyses upon issuance of new external loads is a time-consuming process that can easily last several months. As explained above, such delay in stress substantiations may have a significant impact on the program costs and timeline.

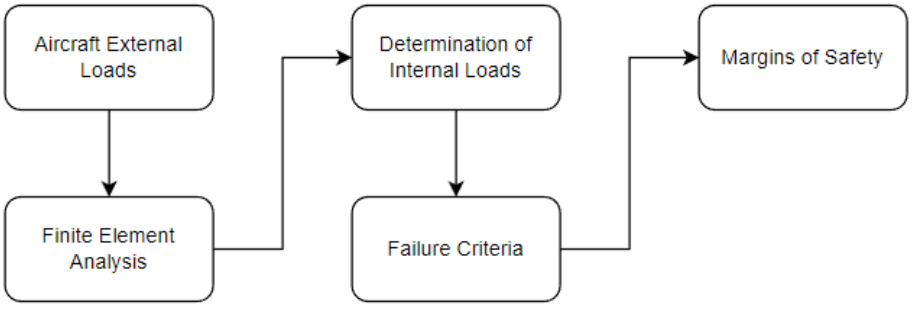

Figure 1: Top level structural substantiation flowchart

The current study proposes a change in the paradigm of how structural details are substantiated. To this end, machine learning strategies are used to significantly enhance the analysis duration, thus providing an assessment tool for the stress engineer to evaluate of a new load loop on the

existing design of the structural detail. The new approach, which is based on machine learning regressions, is presented in Figure 2.

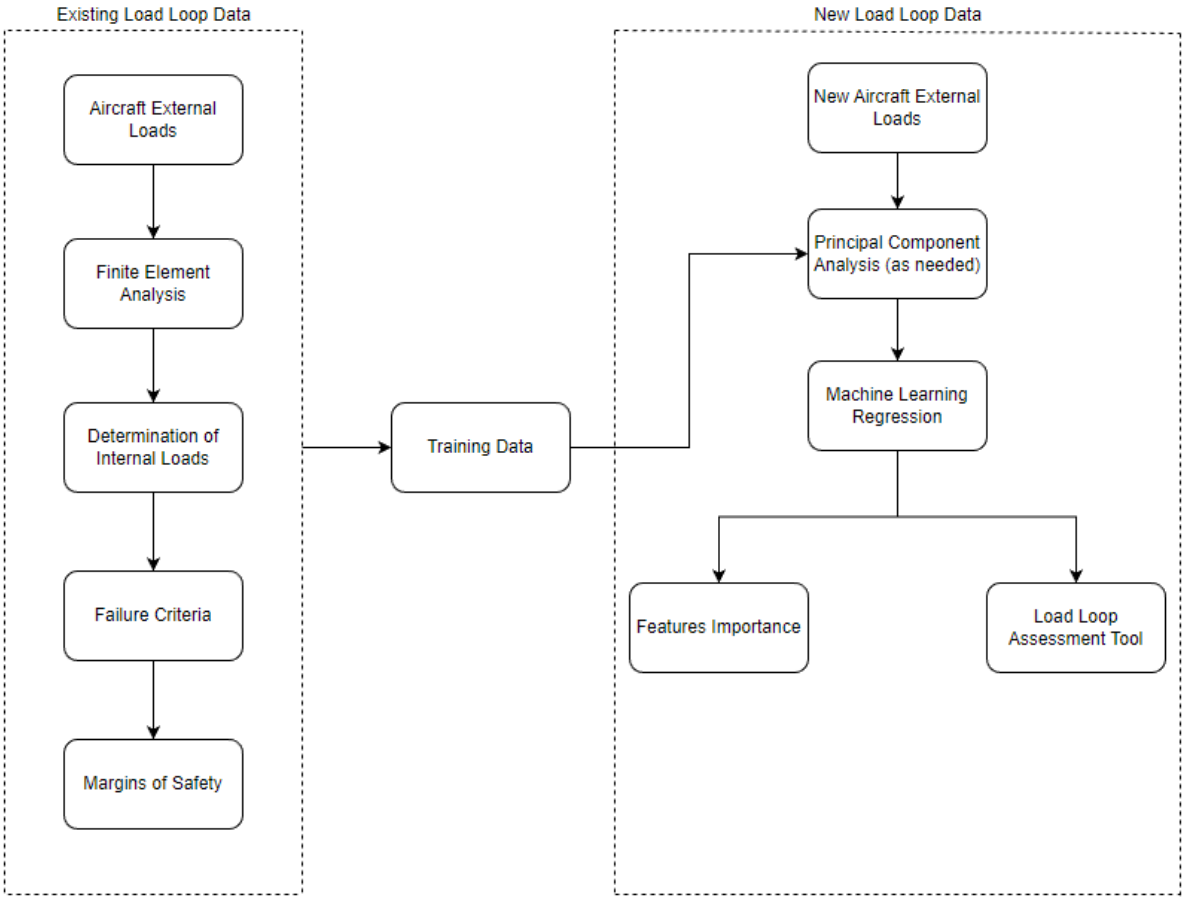

Figure 2: Proposed process for new loads loop assessment

The main idea underpinned by the flowchart presented in Figure 2 is to establish relations between the external loads and the margins of safeties in structural details of concern. This process can be ideally performed analytically in cases when the finite element model and failure criteria are linear. If not, machine learning approaches can be used to establish such relations. Once the algorithm is trained based on the previous external loads loop, predictions of the expected margins of safety can be made for a given new set of external loads using regression. Two outputs are plotted, predictions of the expected margins of safety and evaluation of features importance. Understanding the effect of each feature (i.e., external load component at specific location) is an important tool to support engineering judgement regarding the expected effect of the new loads set on the current design.

Machine learning strategies are used in recent years to address complex technological problems in the field of structural analysis (Refs. 5 - 11 for example). The main advantage of such approaches is their capability to efficiently perform regressions for a given dataset with capability of dealing with large database that includes multiple features.

In this study, the Multilayer Perceptron Neural Network (MLP) and the Random Forest (RF) methods were used. According to the MLP approach, the different features characterizing the problem investigated are represented as neuron with a given weight. These weight functions are coefficients that construct the output signal using summation. An activation process is employed throughout this procedure that maps the summed weights input into the output of the neuron.

Each layer in this algorithm includes a row of neurons, and one network may include several layers. The first layer (the 'visible layer'), represents the input data. The layers after the input layer are the 'hidden layers' since they are a combination of the input layer with their corresponding weights. The final layer is the 'output layer'; The obtained output vector is compared to the training data, and a cost function is obtained. The cost function is minimized by a back-propagating process that optimize the different weight coefficients throughout this process.

Random Forest (RF) is based on set simple random decision trees that are executed in parallel with no mutual interaction. The RF algorithm constructs the outcome of these decision trees and outputs the average (mean) of all individual predictions. Each initial tree includes only a portion of the input features, and with parallel calculations of these decision trees, the regression process becomes a very efficient. This parallel aggregation of the decision trees outputs is called bagging (Bootstrap Aggregation).

The process described in Figure 2 was investigated. To this end, a structural detail that is subjected to 17 load components, with 67 load cases was chosen. 37 critical locations were identified in this structural detail, and margins of safeties were obtained for each of the 67 load cases studied. The data collected construct a large training database of nearly 2,500 data points. 90% of this dataset was used for training, with 10% used for validation.

Figure 3 present the accuracy of the machine learning predictions versus the actual margins of safety. The comparison is normalized as 1/(MS+1), with MS denotes the margin of safety, so that the axis varies between 0 and unity for a positive margin of safety. As can be seen from the graphs presented in this figure, an excellent agreement between predictions and actual margins of safety is achieved, even for relatively small training dataset (recall that the training data includes only 67 load cases; it is expected that larger number of load cases used for training will significantly improve the predictions). The neural network algorithm was found to be superior with respect to the random forest.

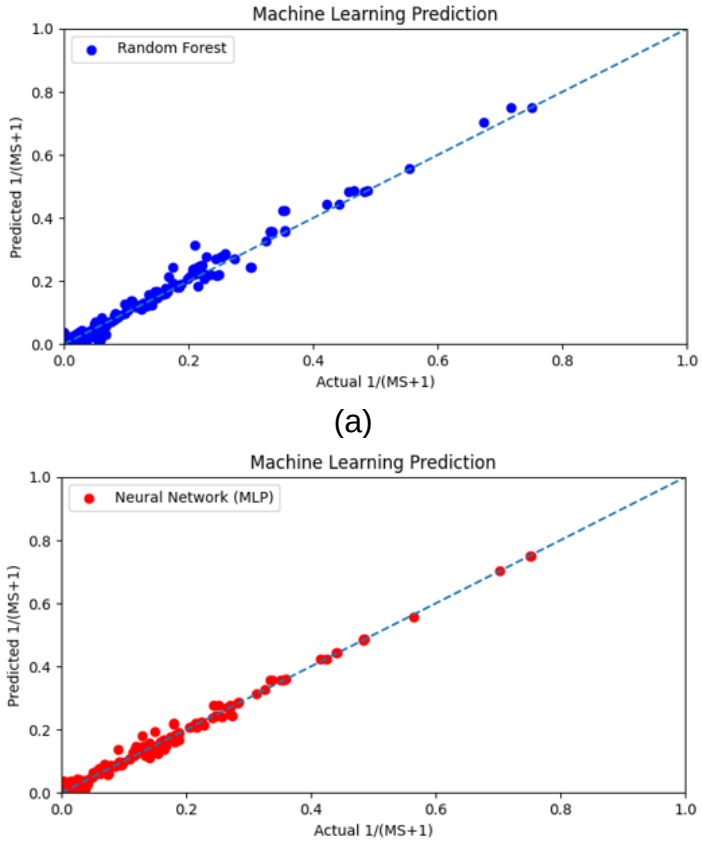

Figure 3: Predictions vs. actual margins of safeties for the validation data. (a) Random Forest and (b) Neural Network

Finally, demonstration of the importance of each individual feature with respect to the obtained margin of safety is presented in Figure 4. Three critical locations are presented, and the components identified as critical were validated via classical stress calculation of the structural detail. Such identification of the importance of each load component is highly important to support engineering judgement that is commonly used for evaluation of new load set.

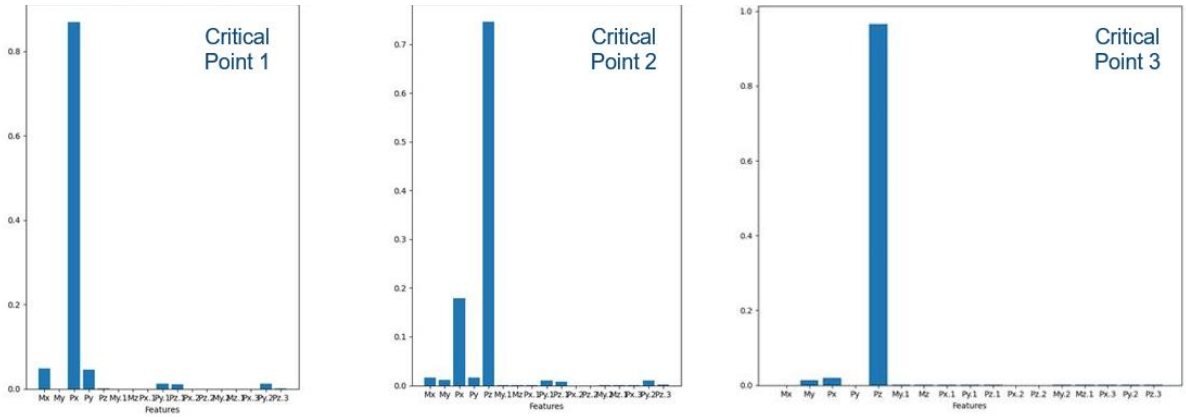

Figure 4: An example of features importance at three critical location

This study was presented in the 62nd annual conference on aerospace sciences [12].

2.2 Three dimensional elliptic and part-elliptic crack fronts (Z. Yosibash, TAU)

The asymptotic solution of the elasticity equations in the vicinity of an elliptical singular edge in 3D was derived and presented explicitly for an elliptical crack with traction free boundary conditions in Ref. 26. It is composed of Edge Stress Intensity Functions (ESIFs), which are functions along the singular edge, eigenfunctions and their shadows. The recursive equations to derive the eigenfunctions and their shadows were provided. The explicit presentation of the series was required to identify the different quantities of interest as the ESIFs and the T-stresses and allows the extension of the quasi dual function method for the extraction of the ESIFs along elliptical singular edge. In Ref. 27, a computational method, known as the Quasi-Dual Function Method (QDFM), was derived for the functional representation of ESIFs along such cracks in 3D domains. It was demonstrated as an efficient post-processing algorithm that may use the finite element solution away from the singular edge.

The T-stress 3D elastic domain containing a straight crack was also investigated. First, the complete asymptotic expansion in the vicinity of the crack front, including the T-stress, was presented explicitly. Having obtained the asymptotic expansion, the QDFM was exploited for the extraction of the T-stress from finite element solutions and express it as a function along the crack front. Since the stress field tends to infinity at the crack front whereas the T-stress remains constant, its extraction from finite element solutions, containing numerical errors, was a non-trivial task. Accurate and efficient methods for extracting the T-stress function along the crack edge by the QDFM was developed. Numerical examples were provided for the computation of the T-stresses from conventional and high order finite element methods in Ref. 28.

Crack initiation in structures made of steel alloys with V-notches at which a small plastic zone usually evolves was investigated recently in two papers (Ref. 29, 30). Failure criteria for predicting fracture loads for such quasi-brittle alloys, as a function of the V-notch opening angle are very scarce and have not been validated by a set of experimental observations. A database of experiments performed on AISI 4340 steel alloy specimens with three different V-notch opening angles and three different tempering temperatures, loaded in mode I, was provided in these studies. Material properties, failure load and plastic area at the V-notch tip were detailed. The experimental observations were used to investigate to which extent the Finite Fracture Mechanics Coupled Criterion (FFMCC) for brittle materials may predict the failure load of quasi-brittle steel alloys, depending on the plastic zone size. Finite element analyses were used to compute the parameters required by the FFMCC. Predicted versus the experimental fracture loads were compared for the different V-notch opening angles and tempering temperatures. For small opening angles (~30◦) for which the plastic area is very small, the FFMCC underpredicted the fracture load by about 20% which is within the experimental error range. The under-prediction of the failure load constantly increased to ~ 50% as the V-notch angle increased to 90◦ and plastic zone area on the surface increases to ~ 0.5 mm^2 (for a V-notch depth of 5 mm). Ref. 29 suggested to be use the experimental database for validation purposes when new failure criteria for quasi-brittle materials are developed. Despite the relatively simple geometry and loading, and the fact that the specimens exhibited small scale yielding, model-based simulations

that can accurately reproduce the critical forces at crack nucleation across the full set of specimens have proven to be elusive. Along these lines, a model-based simulation results from finite-element discretizations of phase-field models for fracture was presented in Ref. 30. Results were provided using both a well-established phase-field model for brittle materials as well as a recently-developed phase-field model for ductile materials. Importantly, both models tie crack nucleation to critical values of energy, and both were shown to be lacking in their accuracy to varying degrees. Standard finite-element calculations of a calibrated plasticity model were also used to demonstrate that much greater accuracy in the calculated critical forces could be obtained with the use of a particular strength envelope.

2.3 Residual stresses in a rotating disk during rotational autofrettage (M. Perl, BGU)

The evaluation of equivalent temperature fields for cylindrical and spherical pressure vessels to imitate autofrettage-induced residual stresses has been successfully implemented in studying crack growth in autofrettaged vessels by the finite element method. Rotational autofrettage is a recent method that can be employed for strengthening hollow disks used in many turbomachinery. The evaluation of the equivalent temperature field becomes pivotal in the performance assessment of autofrettaged cracked disks subjected to high rotational speed. In Ref. 32, an equivalent thermal loading method for emulating the residual stress field in a hollow rotating disk, induced by full or partial rotational autofrettage in a finite element analysis is suggested. An analytical, or a numerical discrete solution, evaluating the equivalent temperature field for an arbitrary axisymmetric residual stress field, induced in a rotating disk due to rotational autofrettage, is developed. This solution is implemented in a finite element analysis to emulate the original rotational autofrettage-induced residual stresses in a typical rotating disk. Applying the equivalent temperature field, the residual stresses obtained in the finite element analysis are further corroborated with the original residual stress field introduced by rotational autofrettage, as shown in Figure 5.

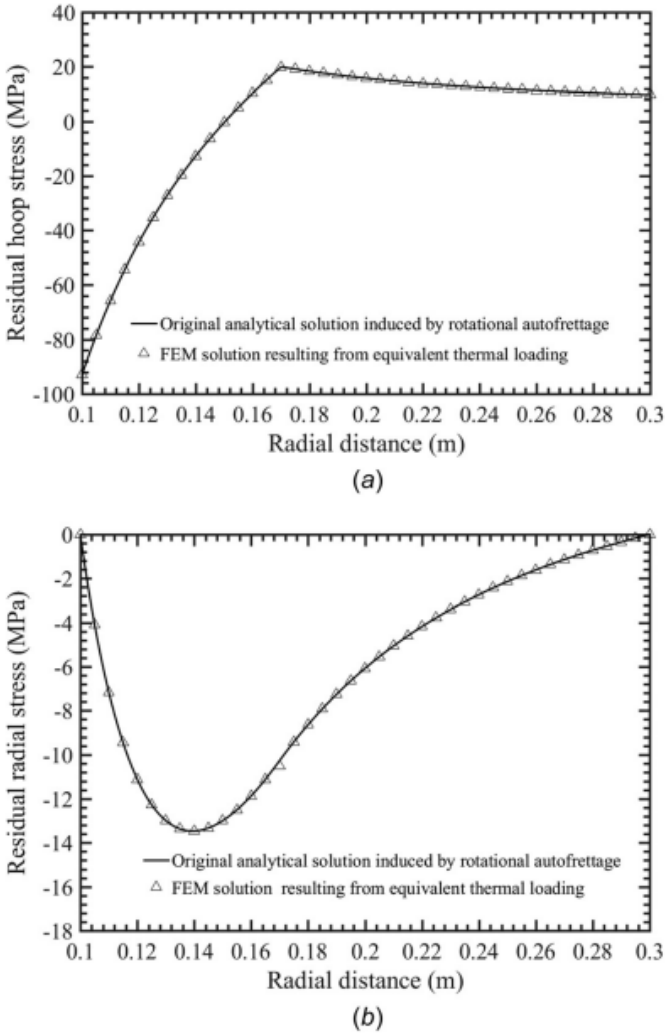

Figure 5: Comparison of the residual (a) hoop and (b) radial stress components in partial rational autofrettage

It is found that the developed equivalent temperature fields excellently reproduce the residual stress fields, within less than 1%, induced by both full and partial rotational autofrettage.

2.4 Internal versus external cracks and their impact on fatigue life of autofrettage tank gun barrels (M. Perl, BGU)

An extensive analysis of the fatigue life of a typical modern autofrettaged smoothbore tank barrel, cracked either internally or externally, in terms of the initial crack depth and shape, type and level of autofrettage, was presented in Ref. 33. Five overstraining cases were considered: no-autofrettage, 70% and 100% hydraulic autofrettage, and 70% and 100% swage autofrettage. The maximum combined stress intensity factors due to both internal pressure and autofrettage, as a function of crack depth for a large number of internal and external crack configurations was determined using finite element analyses. A novel realistic experimentally based

autofrettage model, incorporating the Bauschinger effect, was integrated into the finite element model, replicating both the hydraulic and swage autofrettage residual stress fields accurately. Fatigue lives were evaluated by integrating Paris' Law. It was demonstrated that hydraulic and swage autofrettage have a dramatic beneficial effect in extending the fatigue life of an overstrained barrel (4–11 times as compared to an identical nonautofrettaged tube). Scenarios in which the fatigue life is controlled by internal of external cracking were identified. Eliminating or carefully designing stress concentrators on the tube's external face and keeping away from corrosive agents thus, extending the fatigue-crack initiation life of an external crack, enables the increase of the level of swage autofrettage significantly (swage autofrettage is considered as superior with respect to hydraulic autofrettage). If full swage autofrettage is permissible, the fatigue life of such a barrel is twofold that of a fully hydraulically autofrettaged tube. Unlike the commonly accepted concept, the level of hydraulic autofrettage should not be limited to 70%, and full hydraulic autofrettage should be used. Similarly, in the case of swage autofrettage, if the detrimental effect of external cracking is removed by proper design and maintenance of the tube's outer surface, the level of autofrettage can be significantly increased, thus, gaining an increase of 33% in the fatigue life. Initial crack depth and shape are major factors affecting the fatigue life of the barrel. The deeper the initial crack depth and the slenderer its shape (a/c ratio), the shorter the fatigue life of the barrel.

2.5 Development of new stress intensity factors for nonaligned adjacent cracks subjected to different loading schemes (M. Perl, BGU)

New stress intensity factor solutions for mutual effects of nonaligned multiple cracks were derived in Refs. 34 and 35. An example of such nonaligned cracks is presented in Figure 6. To this end, a case of central and edge cracks subjected to bending loads and three-dimensional quarter circle corner crack combined with internal three-dimensional crack were investigated.

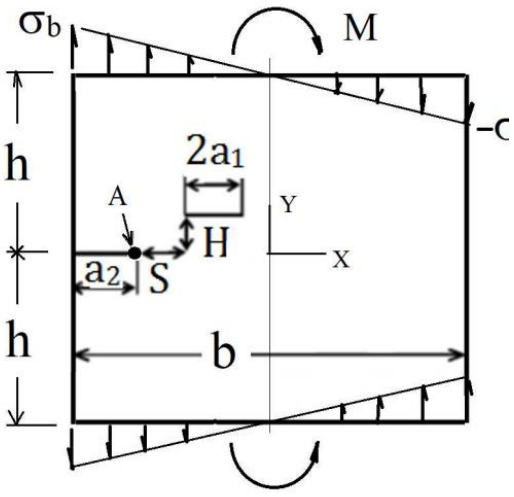

Figure 6: An example of nonaligned adjacent cracks subjected to bending loads

In these studies, hundreds of different cases are solved and the behavior of the SIF distribution along the crack fronts of the nonaligned cracks are assessed when affected by the nearby crack for different geometries and loading schemes. FEM simulation of the mutual interaction between nonaligned adjacent cracks is presented in Figure 7.

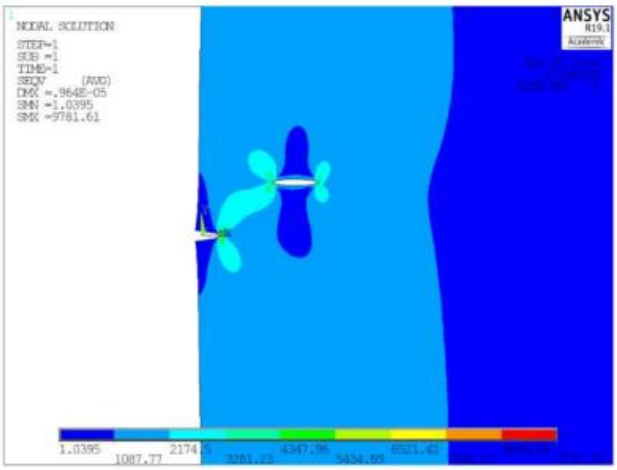

Figure 7: An example of mutual interaction between nonaligned adjacent cracks

2.6 An investigation into curved beam flange efficiency in thin-walled structure (S. Katzeff, IAI)

Allowing a structural member to reach its full loading potential is likely the primary focus of structural analysis. Structural area that is ineffective is seen as 'parasitic', and is eliminated either in the final design iteration, or in a subsequent weight-optimization exercise. The seminal research articles outlining the phenomenon of curved beam flange efficiency were written in the 1950s. Graphs based on seemingly complicated equations are advocated in aircraft structural directives; yet the fundamental mechanism of the true axial stress distribution in an outstanding curved beam flange remains elusive.

In this study, some aspects of curved beam flange efficiency are highlighted. Furthermore, relatively 'simple' linear Finite Element analysis, validated by the aforementioned fundamental research, is shown to adequately capture the phenomenon. Finally, a method is proposed that considers the influence of the corner fillet radius at the connection of the flange to the web, a detail that has not been fully investigated in the literature. The method is outlined for a C section, but can be applied to all thin-walled sections (Z, I and T).

Figure 4: Channel section defining relevant dimensions

The proposed method shows good correlation with current methods found in the literature (for no fillet radius). The proposed method, validated by FE analysis, also attempts to 'recover' some of the efficiency 'lost' by the flange by fully exploiting the increased stiffness afforded by the corner fillet radius, as well as the concomitant reduction of material.

Full length paper of this study is given in Ref. 36.

3. STRUCTURAL INTEGRITY OF COMPOSITE STRUCTURES

3.1 Mixed mode failure predictions of adhesively bonded joints based mixed mode bending testing (Y. Freed and A. Levi Sasson, IAI)

Using bonding as an assembly method to join large composite components has the potential to be very effective from almost every perspective. Such process features low weight design and can demonstrate a dramatic reduction in assembly effort (parts and fasteners count) and related costs. However, bonded joints often characterized with low bond strength, that may be resulted from improper surface preparation, bond-line contamination, high humidity or insufficient control of cure temperature. This low strength bonding is undetectable since to date, there is no reliable Non Destructive Inspection (NDI) technique available to adequately ensure that a bonded assembly has retained its full strength. Therefore, the current certification standards require that:

"*…the maximum disbonds of each bonded joint consistent with the capability to withstand the loads… must be determined by analysis, tests, or both. Disbonds of each bonded joint greater than this must be prevented by design feature…*"

The above mentioned regulatory requirement emphasizes the challenges in insertion of bonded composite joints design to certified aviation products.

This study proposes a failure criterion for the EA 9394 paste adhesive which is commonly used for assembly of large components in the aviation industry. The data used to determine the failure model is based on Mixed Mode Bending (MMB) testing. Such testing protocol is basically a combination of the Double Cantilever Beam (DCB) test used to obtain mode I failure characteristics, and the End Notch Flexure (ENF) method that is used to characterize mode II failures. The mode mixity is reached by changing the position of the MMB lever, as is schematically shown in Figure 8.

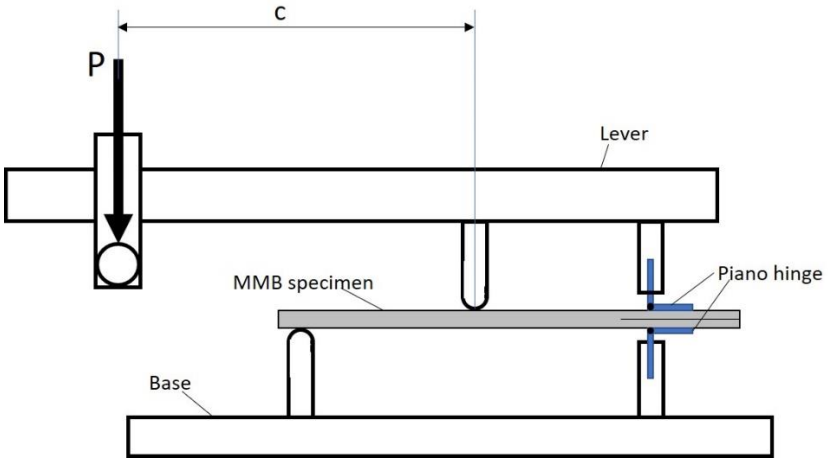

Figure 8: MMB test fixture. The mode mixity is controlled by changing the loading position (dimension 'c' in this sketch)

The test specimens were assembled from unidirectional composite adherents made of Hexply 913 pre-impregnated resin system with standard modulus fibers. The adherents' layup was $[0°]_{16}$, with ply thickness of 0.125 mm. The adherents were cured at 125°C (257°F) before bonded together using Loctite EA 9394. The curing of the bonded specimens was conducted for five days at 25°C. A vacuum bag was used to remove air voids and improve bonding. The specimens dimensions are $2L = 110$ mm, $d = 2$ mm, and $t_a = 1, 2$ and 3 mm. The initial disbond length, a, was measured for each specimen, and is generally spanned between 10 – 35 mm. The test specimens were mounted in the MMB test rig and the mode mixity was reached by defining the lever position, c, as required. All tests were conducted in ambient conditions, under displacement-controlled loading. Figure 9 presents the fracture energies obtained in these tests as a function of the adhesive thickness and the mode mixity.

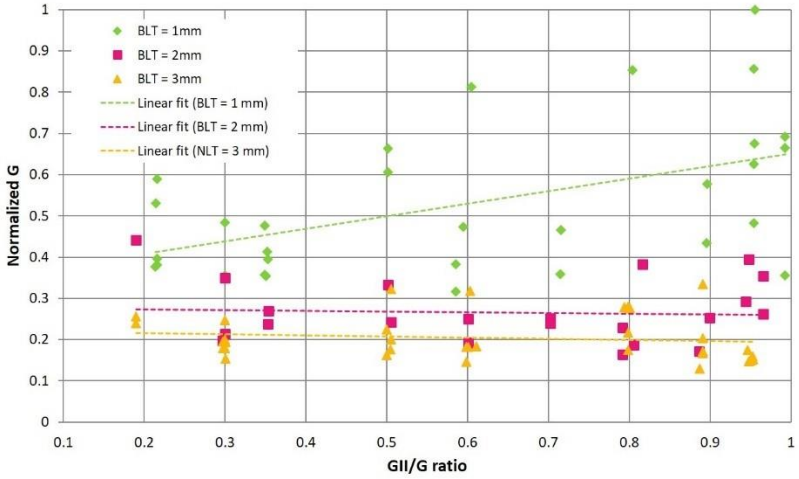

Figure 9: Summary of test results (normalized total energy release rate to mode mixity ratio) for all specimens tested

Based on these test results, failure criterion was established. The proposed failure criterion in this study is a von-Mises like failure criterion:

$$\left(\frac{\sigma}{\sigma_{ult.}}\right)^n + \left(\frac{\tau}{\tau_{ult}}\right)^m = 1$$

Where σ and τ are the tensile and the shear stress obtained by FEM at the disbond tip, σ_{ult} and τ_{ult} are the strength for pure tensile and pure shear conditions, and n and m are constants that were calibrated from the test results.

Finite element models were constructed to obtain the shear and tensile stresses in the vicinity of the disbond tip. Based on these analyses, failure envelopes were obtained, as shown in Figure 10.

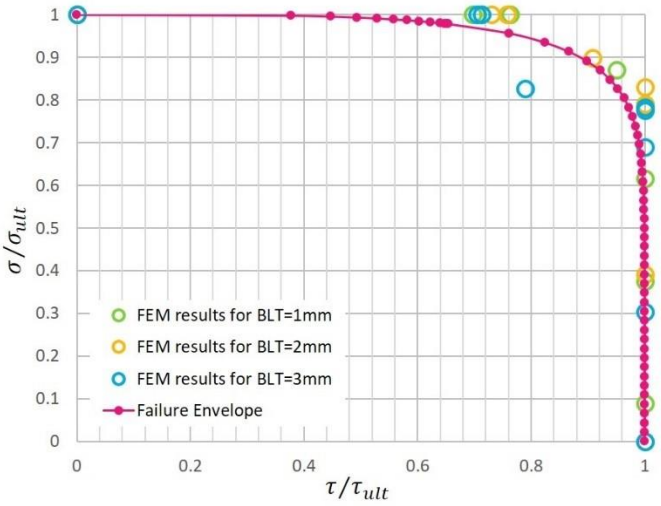

(a)

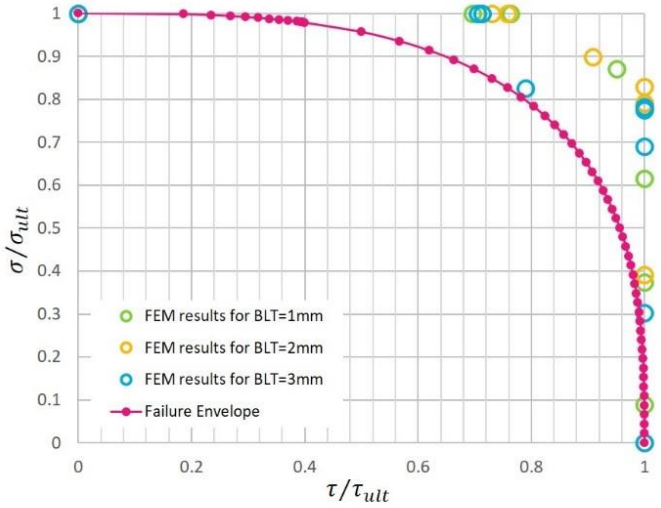

(b)

Figure 10: Normalized failure envelope for 9394 adhesive with different bond line thicknesses. (a) optimized correlation to test data with m = 4.04, n = 9.06 and (b) conservative envelope that can be used for design with m = 3.0 and n = 3.0

A full length paper describing this study was submitted for publications [2].

3.2 Development of aviation industry-oriented methodology for failure predictions of brittle bonded joints using probabilistic machine learning (Y. Freed, IAI)

Composite materials are increasingly used in the aviation industry over the last half century, given their high specific stiffness and strength ratios. Using composite materials for primary structure introduces several engineering challenges, such as real time monitoring of fabrication defects, quality assurance management, sensitivity to environmental conditions and impact damages, efficient design, suitable tooling and more. From the assembly point of view, attachment of cured composite parts using fasteners requires careful design that accounts for various aspects such as layup orientation for suitable fastener bearing strength, local pad-ups to avoid knife-edge scenarios, and sufficient access for drilling and fasteners installation, whether performed manually or automatically. Alternatively, bonding cured composite parts (even large critical structures such as pressure hulls and wing box structures) have the potential to be very effective from almost every perspective. Such assembly process features a low weight design and may lead to a dramatic reduction in assembly effort and related costs compared to bolted joints. Lockheed Martin demonstrated this a few years ago during the development of the Advanced Composite Cargo Aircraft (ACCA), in which a Dornier 328J (DO-328J) aircraft was used as a benchmark. In the ACCA (or the X-55 aircraft), advanced composite materials were used in the fuselage and vertical tail to replace the original DO-328J metallic design (approximately 40% of the total air-vehicle parts were replaced). significant reduction in part count were reported, leading to a significant recurring cost reduction.

The main drawback of using paste adhesives as an assembly process is that bonded joints still require a very strict processing control to ensure sufficient quality for the specific materials and processes used for a given structure. The main concerns are issues such as improper surface preparation, bond-line contamination, high humidity, and insufficient control of the cure cycle. These may lead to undetectable low bond-line strengths, usually refer to as "kissing bonds". This risk was highlighted in 2005 when an Airbus A310 aircraft lost its rudder (made of co-bonded sandwich structure) during flight due to weak bond-line between the substructure and its outer skins [13]. Another relevant accident is a case of a 7 feet separation of a wing skin to main spar bond-line in a Cessna Corvalis aircraft during flight test in December 2010. The FAA investigation revealed quality assurance failures in the manufacture of the wings of the damaged airplane [14]. As of yet, no reliable Non Destructive Inspection (NDI) technique is available to adequately ensure that a bonded assembly has retained its full strength ([15]-[16]), although some progress was reported recently [17]. Therefore, the current certification standards ([18]-[21]) require the investigation of the maximum disbonds of each bonded joint. This should be consistent with its capability to withstand expected limit loads. The determination of maximum disbond size must be conducted by analysis, tests, or both. Disbonds that are larger than the allowed size must be prevented via design features such as rivets.

The objective of this study is to propose a new industry-oriented methodology to determine failure parameters to predict the residual strength of adhesively bonded joints. Such approach can be adopted by the aviation industry if the failure criterion is relatively simple, does not require large amount of failure parameters to be calibrated and is already implemented in

commercial software, so failure predictions can be made to large scale assemblies. The proposed methodology includes implementation of machine learning strategies to analyze a great amount of physical test data and simulation data to calibrate the failure parameters of the Virtual Crack Closure Technique (VCCT) and the Cohesive zone Model (CZM). Calibration of these failure criteria using machine learning strategy allows the designer to determine the maximum allowed disbond size for each assembly. Knowledge of the maximum allowed disbond size is an important step towards certification of bonded composites in commercial products.

Figure 11 presents the methodology employed in this study. The test data presented in Section 3.1 was utilized. Thousands of finite element models were constructed, each differs from the others by the set of failure parameters used for CZM and VCCT failure predictions. Next, the Gaussian Process Regression (GPR) machine learning algorithm was employed to obtain the optimized failure parameters for each failure criterion. Statistical analysis was conducted to ensure sufficient reliability and confidence in the predictions. Finally, the failure predictions were validated with respect to element level bonded structures.

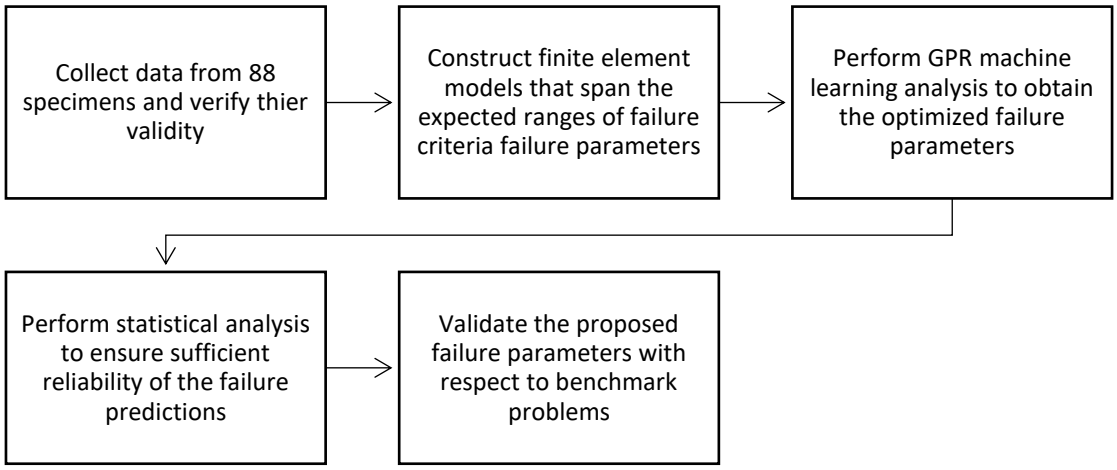

Figure 11: Methodology to obtain VCCT and CZM failure parameters

The outcome of this process is presented in Figure 12. These figures refer to the failure predictions using the VCCT method.

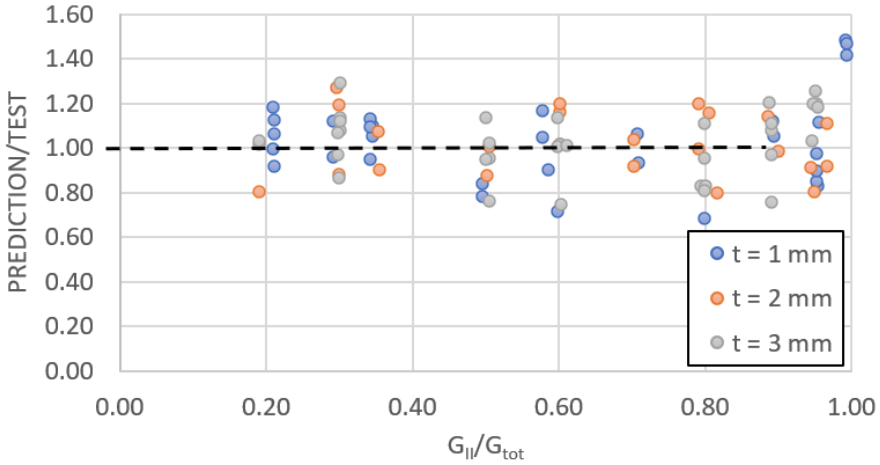

Figure 12: Comparison between predictions and test results for all 88 specimens. The predictions/test values are shown as a function of the mode mixity G_{II}/G_{tot}

As can be seen from Figure 12, the predictions are generally accurate with respect to the test data for all 88 specimens, but large scatter is reported. To ensure sufficient reliability and proper confidence in the failure predictions, statistical analysis is performed. The values of prediction/test were fitted assuming a Weibull distribution, as presented in Figure 13. B-Basis failure parameters were obtained using two methods. First, the B-Basis limit was obtained from the Weibull fitting curve and a safety factor was defined as the ratio between the B-Basis limit and the average. An alternative approach for determination of safety factors is to evaluate failure parameters that will lead to failure predictions which are conservative for at least 90% of the test articles population with confidence level of 95%. This can be easily achieved by performance of machine learning analyses but with different cost function.

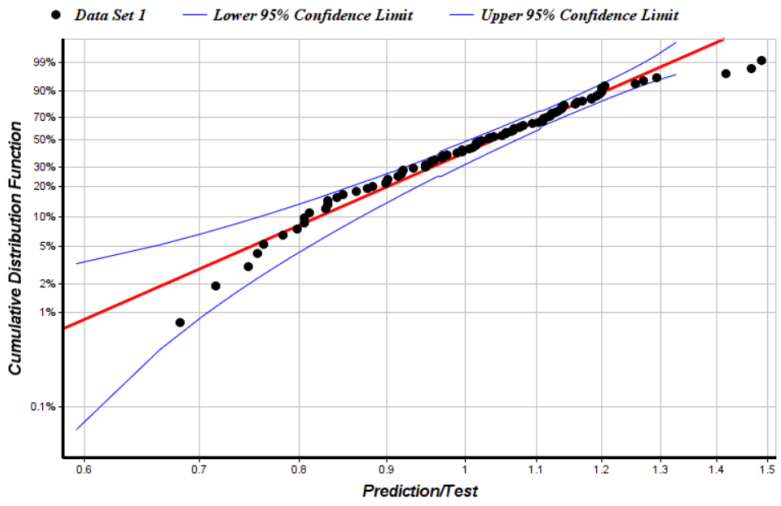

Figure 13: Weibull distribution fitting of Prediction/Test values for all 88 test specimens. The predictions assumed VCCT fracture parameters of G_{Ic} = 0.33 N/mm, G_{IIc} = 0.37 N/mm, n = 3 obtained by pooling test results from all adhesive thicknesses

The proposed methodology was validated using several element level test results. An example of such validation is presented in Figure 14. Thick adherents lap joints were used. Average

CZM failure parameters were used for the predictions. The ratio between the predictions and the test results vary between 0.93 to 1.29, depending on the adhesive thickness. The relatively large difference between the predictions and the test results for adhesive thickness of 3.49 mm can be explained by the fact that adhesive failures (and not cohesive failures) were reported for this thickness in tests, leading to failure in tests earlier than expected. Usage of B-Basis CZM failure parameters maintain the predictions as conservative even for this adhesive thickness.

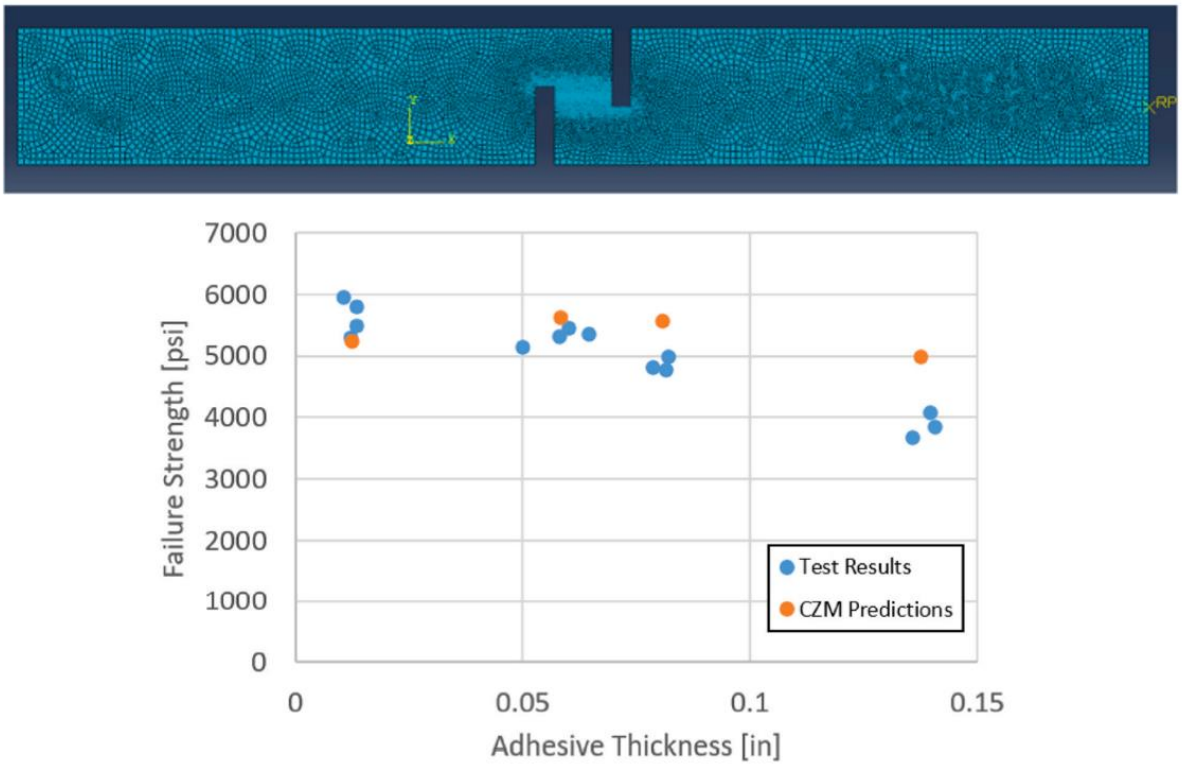

Figure 14: Bonded lap joint validation demonstration – test results vs. CZM predictions

This study is summarized in two journal papers ([9], [10]), each dealing with different failure criterion.

3.3 Implementation of machine learning strategies for determination of finite width correction factors for orthotropic plates containing central hole (Y. Freed, IAI)

The design of primary structures made of composite materials is governed by damage tolerance allowables, as guided by the relevant regulation requirements for both military and civil products. That is, the design must be tolerant to imperfections at the composite structure that may be introduced during manufacturing, assembly or service. An industry practice for determination of damage tolerance allowables is the Open Hole Compression (OHC) test protocol. According to ASTM D6484 standard, the ratio between the specimen width W and the open hole diameter D is W/D = 6. However, the design of structural parts often limits the edge distance of fastener holes, leading to ratios of W/D which are below 6; for this case, the strength allowables determined by the OHC testing scheme should be adjusted by application

of a finite width correction factor. As opposed to metallic structures, the laminate layup plays a major role affecting the strength allowables when finite width correction factor is considered.

In this study, machine learning strategies are employed to predict the finite width correction factor of orthotropic plates. Machine Learning (ML) algorithms have been used to study different characteristics of composite materials in the past few years [7]-[11]. The main advantage of using such approaches over standard numerical analyses is their capability to efficiently perform regression based on relatively small dataset. ML approaches can also deal with large data very efficiently. While there are many ML strategies available, they all similar to each other in their regression process. As a first step, the algorithm is 'trained' with respect to a given dataset. In this process, the algorithm establishes correlations between the different data points with respect to predefined characteristics. It is strongly recommended to use a physical-based model for the training procedure, especially if the training process is based on relatively small dataset. Once these relations are established, the entire investigated domain can be spanned using regression.

Several machine learning algorithms were utilized in this study to obtain finite width correction factors for IM7/8552 unidirectional composite material. The proposed methodology also includes a procedure to determine the number of required training data points using the Gaussian Process Regression (GPR) algorithm. Finite width correction factors carpet plots were produced, allowing the designer to easily obtain the required correction factor for a given layup and geometrical characteristics. An example of such carpet plots for W/D = 3 is presented in Figure 15.

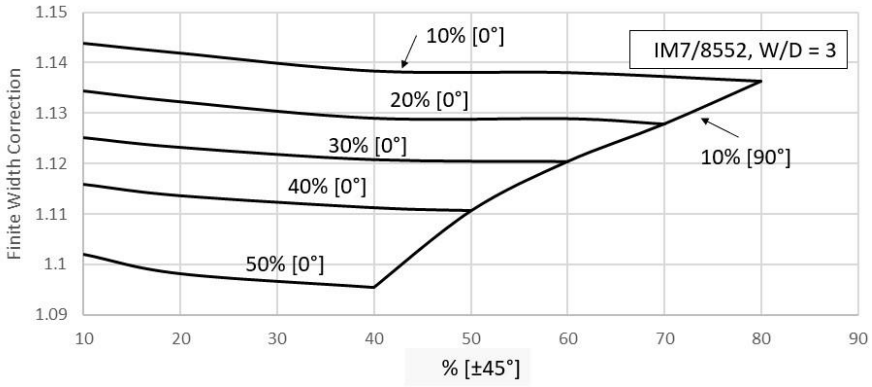

Figure 15: Finite width correction factor carpet plot for IM7/8552 with W/D = 3

The finite width correction factors were validated with respect to test data [22] at several ratios of W/D. The performance of three machine learning was evaluated Gaussian Process Regression (GPR), Multi-Layer Perceptron (MLP) and Random Forest (RF). As can be observed from Table 1, excellent agreement is achieved with less than 4% error for all machine learning algorithms studied here.

Table 1: Validation of machine learning predictions versus test data (IM7/8552, Quasi-Isotropic layup, hole diameter of 5 mm)

	Finite Width Correction Factors						
W/D	Test Data [22] D = 5 mm	GPR	Error GPR [%]	MLP	Error MLP [%]	RF	Error RF [%]
6	1.00	1.00	0.0%	1.00	0.0%	1.00	0.0%
5	1.02	1.01	-0.5%	1.03	0.8%	1.01	-0.7%
4	1.05	1.06	0.5%	1.07	2.0%	1.05	-0.1%
3	1.15	1.12	-2.3%	1.11	-3.5%	1.12	-2.3%

This study was summarized in a journal paper [11] and will be presented in the 31st ICAF symposium.

3.4 **Characterization of the mechanical response of composite poltrusions (Z. Yosibash, TAU)**

Ref. 31 focuses on pultrusions, which have constant cross-sections of unidirectional composites with a significant long length. The mechanical response at three modes of loading was studied: tensile, compression, and shear loading of coupons made from a graphite/epoxy 1 mm sheet. In addition, the effects of holes and notches were examined in terms of mechanical properties. The mechanical behavior was assessed through stress–strain curves with careful attention on the curve profile, macroscopic fracture modes observations, and optical microscopic tracking with continuous video records. Finite element analysis (FEA) was used to accurately determine the shear modulus, and for other mechanical investigations. By nature, under tension, the unidirectional fiber composite at 0-orientation exhibited high strength (2,800 MPa), with very low strength at 90-orientation (40 MPa). Both orientations displayed linear mechanical behavior. Under compression, 0-orientation exhibited low strength (1,175 MPa), as compared to tension due to the kinking phenomena, which was the origin in the deviation from linear behavior. Under shear, both orientations exhibited approximately the same shear strength (45 MPa for 0 and 47 MPa for 90), which was mainly related to the mechanical properties of the epoxy resin.

In general, in the presence of holes, the remote fracture stress in the various modes of loading did not change significantly, as compared to uniform coupons; however, some localized delamination crack growth occurred at the vicinity of the holes, manifested by load drops up to the final fracture. This behavior was also attributed to the tension of notched coupons. FEA showed that the shear values were unaffected by manufacturing imperfections, coupon thickness, and by asymmetrical gripping up to 3 mm, with minor effect in the case of a small deviation from the load line. Selected experimental tests support the FEA tendencies.

3.5 Predictions of mode I fatigue propagation properties for MD laminate composites containing arbitrary fiber orientations using machine learning Tools (M. Mega, Ariel University)

In recent years, the aerospace industry has seen a surge in the use of carbon fiber reinforced polymers (CFRPs) due to their lightweight and strong properties. However, the lack of failure criteria for laminated CFRP composites can result in catastrophic failures, particularly delamination between plies. Consequently, extensive testing is necessary to determine the fatigue failure properties of such composite laminates. In addition, multi-directional (MD) laminates may exhibit varying fatigue failure properties depending on the fiber orientations within each ply. Therefore, testing is crucial for accurately characterizing the fatigue failure properties of each designed layup. To reduce the number of tests required for new MD orientations, this investigation aims to establish a relationship between various MD interface orientations and fatigue characterizations.

Seven MD composite laminates made from seven varying layups, each containing initial delamination along a specified interface were tested under mode I displacement control fatigue. For each layup, fatigue delamination propagation rates (da/dN) were determined and plotted against the maximum energy release rate (G_{Imax}) for each cycle. Two different methods were used to evaluate the energy release rate, namely the local J-integral which is performed with numerical finite element analyses (FEAs), and the global modified compliance calibration (MCC) method.

The test data was fitted to a Paris-like equation form. Similar slopes 'n' were exhibited for both analysis methods. However, a shift between the plots obtained via local and global methods was observed for all interfaces (Figure 16). The cause for this shift is currently being investigated and perhaps may be related to the complex energy dissipating mechanisms that occur during propagation, namely fiber bringing, delamination migration, etc. Based on these results, it may be concluded for now that the MCC analysis produced more conservative values.

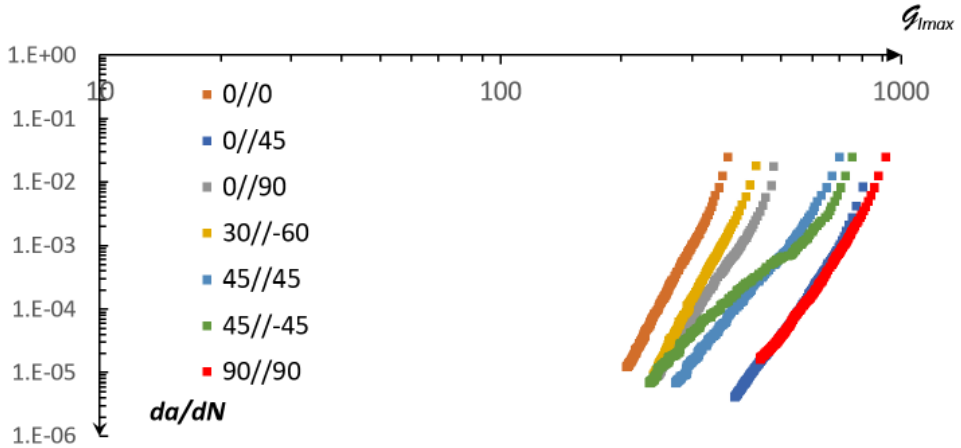

Figure 16: Delamination extension rate versus MCC energy release rate for seven different MD interfaces

The resulting analyzed curves are now employed to train machine learning algorithms (MLAs), which will enable the predictions of the fatigue characteristics for additional arbitrary ply orientations and interfaces. In addition, a relationship between fatigue behavior and the ply orientations will be established.

3.6 Design and experimental validation of a bonded structure fail-safe damage arrest concept (D. Bardenstein, IAI)

The need for light-weight and cost-effective fiber reinforced airborne primary structures drives the industry towards more integral design concepts. Adhesive bonding is increasingly employed as an attractive alternative to mechanical fastening. Aside from the weight reduction due to elimination of fasteners, the high stiffness of bonded joints and the smooth load transfer they provide, are major advantages of this concept. However, the lack of reliable bonded-joint damage-growth analysis combined with the inadequacy of commercially available non-destructive inspection methods to evaluate the strength of bonded joints – has inhibited full adaptation of such joining concepts.

This study presents a fail-safe crack arrest concept for bonded joints in order to ensure predictable slow damage growth. The US department of defense joint service specification guide No. JSSG-2006 for aircraft structures outlines the nature and the certification approach for fail-safe crack arrest structures (section 6.1.21) as

"*crack arrest fail-safe structure is structure designed and fabricated such that unstable rapid propagation will be stopped within a continuous area of the structure prior to complete failure. Safety is assured through slow crack growth of the remaining structure and detection of the damage at subsequent inspections. Strength of the remaining undamaged structure will not be degraded below a specified level for the specified period of unrepaired service usage*".

This study introduces the Mushroom Damage Arresting Feature (MDAF) concept that has developed for a typical stiffened panel and was successfully demonstrated in both Mode I (tensile mode) and Mode II (shear mode). Fatigue test results showed that the MDAF concept demonstrated controlled and slow damage propagation. Significant number of load cycles were needed to propagate the dis-bond through each of the mushroom's pair features.

This study will be presented in the 31st ICAF symposium.

3.7 OPTICOMS - Optimized Composite Structure for Small Aircraft (A. Sawday, IAI)

Playing an important role within IAI's strategic R&D activities, OPTICOMS is one of several projects within the EU's comprehensive R&D program; Clean Sky 2, in which IAI is not only a participant, but a project leader.

As part of the Airframe module, OPTICOMS is centered around the improvement of aerostructures, namely a wing in the FAR23 class. More specifically, the technical goals of OPTICOMS is to develop an expansive, innovative methodology for low cost, automated composite material aerostructure design, manufacture and substantiation for low volume production.

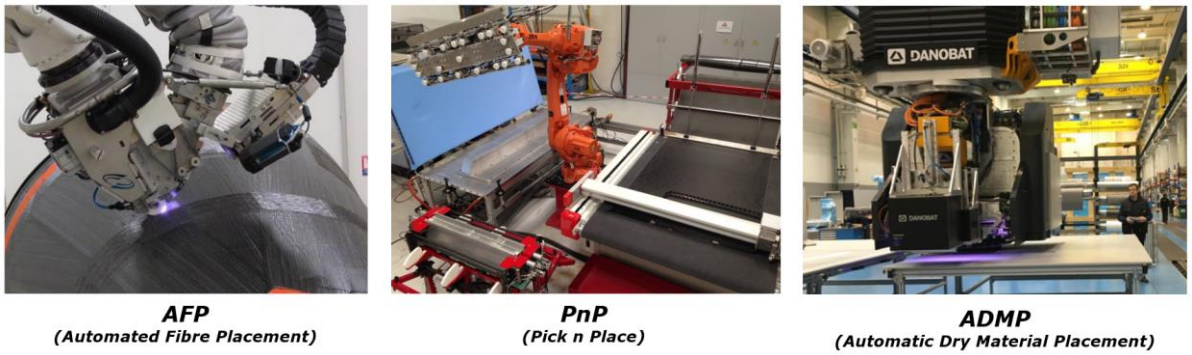

Figure 17: Automated composite manufacturing technologies being assessed in OPTICOMS

Ambitious targets include reductions in production, design & certification and life-cycle costs, along with reduced structure weight. As a means of achieving these targets, key strategic technical guidelines have been defined that include:

- Automated composite manufacture
- DTC (Design to Cost) for low volume production
- Integral structure
- OoA (Out of Autoclave) processes & materials
- Structural bonding

Using the metallic wing of Piaggio Aerospace's P180 Avanti as the baseline, the OPTICOMS consortium (which eventually included over 15 independent European companies) was tasked with producing and substantiating a full-scale, 7m half-wing composite demonstrator. This entire process included the definition, conceptualisation, design, manufacturing (including building block pyramid coupons to elements), finally culminating in a static ground test (as illustrated in Figure 19).

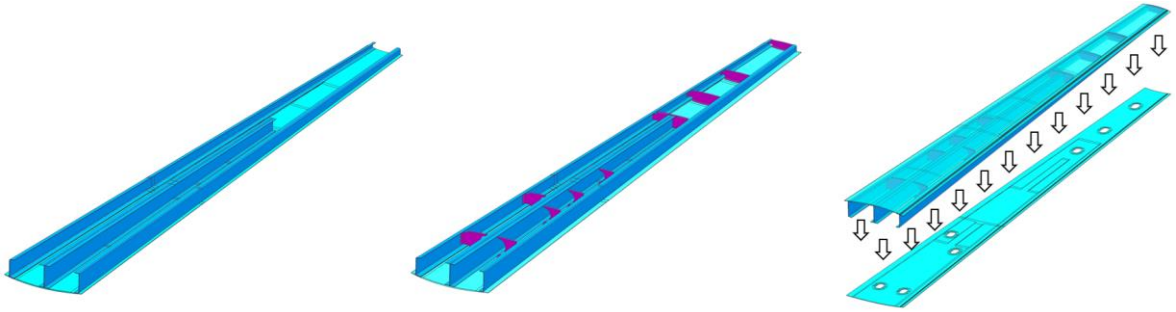

Figure 18: Major manufacturing stages (i) Co-cured skin and spars, (ii) Ribs installation, (iii) Lower skin bonding

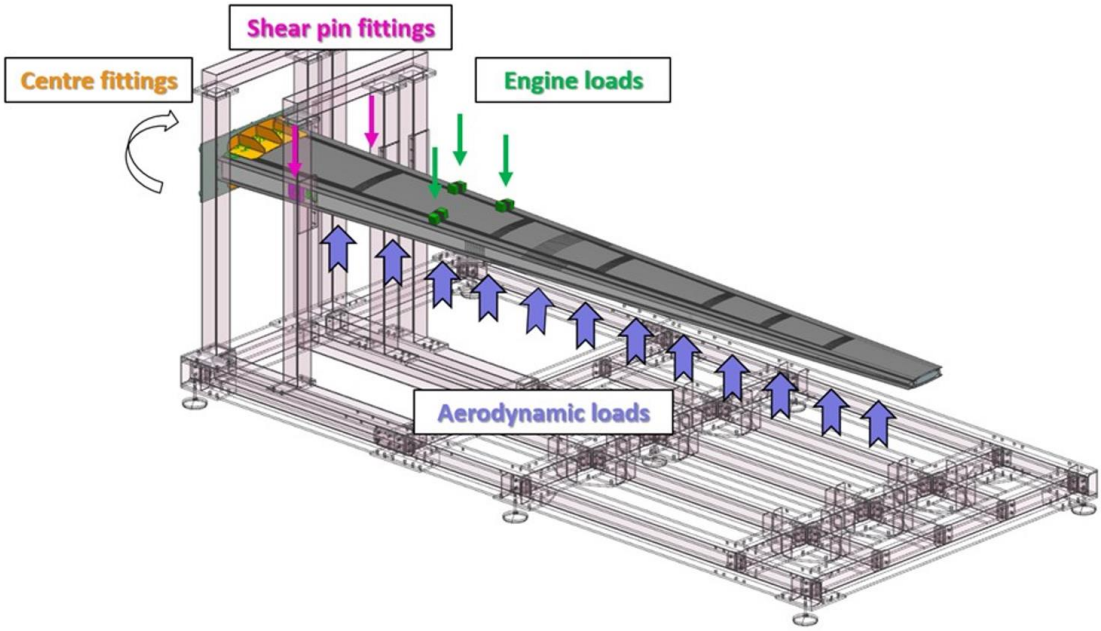

Figure 19: Final static ground test scheme

The project includes supporting activities such as characterization of bond-line strength and failure predictions (as described in Section 3.1), and structural health monitoring of bond-line using optical fiber based sensing technology, all towards future certification of bonded composites.

Currently in the final stages of assembly, all major components have been manufactured, including the challenging layup and infusion of the 7m integral wing-box, which includes the upper skin and 3 spars, all co-cured.

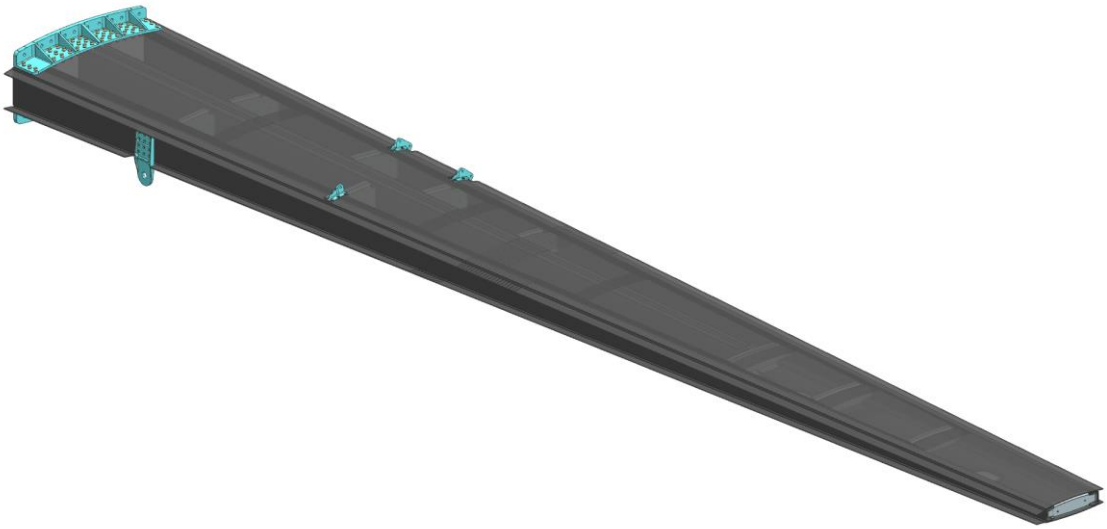

Figure 20: Final 7m wing demonstrator

Figure 21: Final demonstrator integral wing-box infused component

The ribs are currently being bonded, soon to be followed by the lower skin

Figure 22: Assembly/Bonding jig

Upon completion of the lower sin bonding and attachment of all fittings, the demonstrator will be sent to its final destination in Italy, to undergo a comprehensive validation phase, consisting of:

- Static test to LL
- Introduction of BVID
- Fatigue test
- Static test to UL
- Introduction of VID
- Residual strength test (damage tolerance)

4. STRUCTURAL HEALTH MONITORING

4.1 Anomalies detection during full scale fatigue test using machine learning approaches (Y. Freed, IAI)

The development of modern air-vehicles is a harmonized activity of numerous disciplines, such as aerodynamic sciences, propulsion, materials science, structural analysis, systems, avionics, manufacturing and more. The airframe design is based on data provided from these disciplines (for example, updated loads, weight, mass distributions and more). These data are usually provided to the designer in predetermined milestones that are correlated to logistic considerations (such as manufacturing preparations or purchasing of long lead items), all in light of the expected entry to market date.

Full scale fatigue test is a routine procedure that is conducted during the development of new air vehicles. As part of this test, a structurally complete airplane is used as a test article and is fatigue tested for several design life goals. Fatigue loads are applied to the test article through several dozens of loading jacks with cabin pressure simulated as needed. Full description of a full-scale fatigue test of a business jet is provided in Refs. 23 and 24.

A full-scale fatigue test has several objectives. Its main objective is to demonstrate the structural integrity of the aircraft airframe with respect to its design life goal. In addition, this test is commonly used to validate crack initiation and crack growth predictions that are conducted as part of the structural substantiation campaign of the airplane. The validation process also includes validation of non-destructive techniques that will be used for crack detection in maintenance checks during service.

Typical full-scale fatigue test duration is several years. It is commonly completed years after the first airplanes are delivered to the customers. Any fatigue cracking detected in early stages of the test should be addressed, and design changes to preclude such cracks are introduced. While such design changes can be easily implemented for serial production, retrofits to preclude fatigue cracking in airplanes that are already in service are extremely costly. Such retrofits are usually associated with removal of the aircraft interior and installation of reinforcement as needed. Each repair can easily cost several tens of thousands of dollars (including the airplane down-time for repair), and implementation of such repairs in fleet of several dozens of aircraft (that were already delivered to the customer prior identification of fatigue cracks in the full-scale fatigue test) can reach millions of dollars.

The motivation of early detection of cracks during full scale tests is thus clear. There are two techniques that are commonly used to detect cracks in such tests. First, non-destructive inspections are scheduled periodically [23]. During these inspection periods, technicians inspect the test article airframe at pre-defined locations for cracks. Secondly, strain gauge measurements are recorded at specific load cases (for example wing bending or cabin pressure). It is expected that once a crack is initiated in the airframe, the loads will be redistributed in the

structure, leading to changes in the readings of strain gauges. As discussed in Ref. 24 for example, a total of 1,350 strain gauges were used in a recent full-scale fatigue testing of a business jet.

The objective of this study is to propose new approaches for anomaly detection in full scale fatigue tests, acknowledging that early detection of cracks during test may save hundreds of thousands of dollars. Since large data is needed to be analyzed, machine learning algorithms for anomalies detections are exploited to achieve this goal. Machine learning algorithms are increasingly used recently to overcome technological challenges in the field of structural analysis [5 - 12]. Their main advantage is their capability to efficiently perform regressions for a given dataset with ability of dealing with large database that includes multiple features. Such approaches can also be used for classification and anomalies detection [25].

Several anomalies detection algorithms were employed. For example, as illustrated in Figure 23, an anomaly detection algorithm was employed individually for each strain gauge. To this end, after phase of data preparation, samples from the last 10 calibration events were accumulated and statistically analyzed. Upon new measured strain at a given strain gauge, an anomaly criterion was evaluated, and if it was met, the algorithm flags the strain gauge as prone to anomaly.

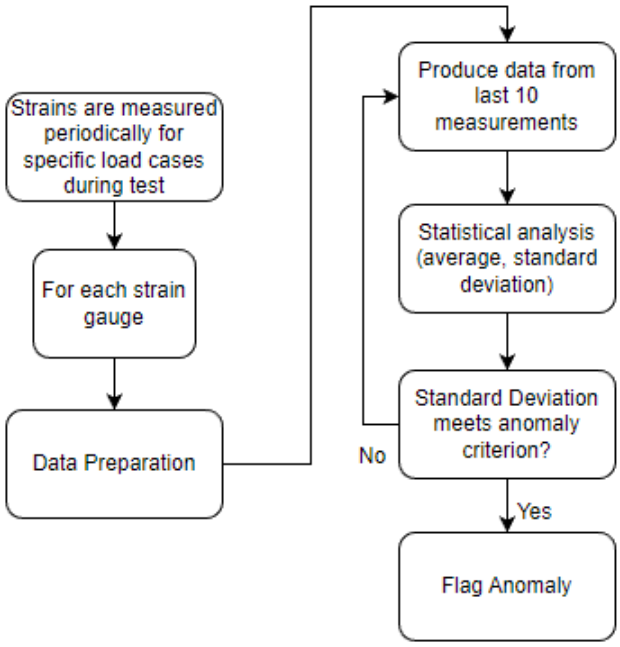

Figure 23: Flow-chart describing anomalies detection technique during full scale fatigue test

A general overview of the anomalies detected during test using the approach described above is shown in Figure 24. The Y-axis in this graph denotes the test progress in terms of flights (up to 50,000 flights). The X-axis summarizes data from roughly 600 strain gauges. The scale changes from negative to positive unity, with positive unity (highlighted in white color in this

sketch) denotes anomaly that was detected in a given strain gauge during test. It is clearly observed that at certain locations during test (~ 18,000 flights for example), many strain gauges reported anomalies. Indeed, major repairs were conducted in the test article at this point in test.

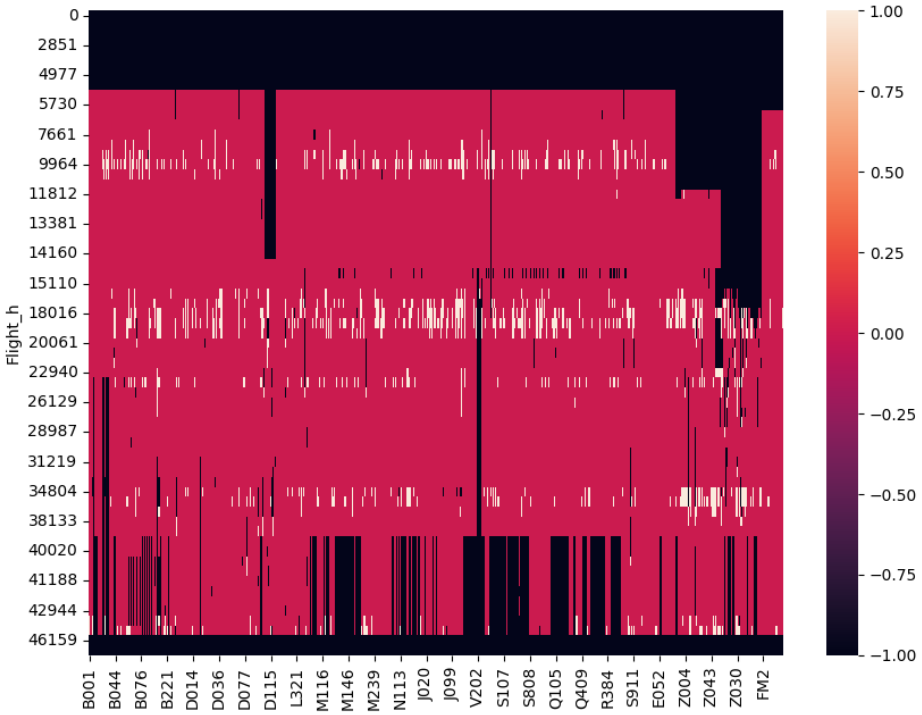

Figure 24: A qualitative illustration of the anomalies detected during test

Other machine learning algorithms were employed to analyze the data collected from strain gauges in test. For example, since the strain gauge measurements are recorded at specific load cases, if the test article is intact, linear correlations between different events in which the strains were measured can be postulated. Usage of the Principal Component Analysis (PCA) on such data will reduce this n-dimensions problem (in this case, n is the number of strain gauges, ~ 1,350) to a single dimension problem. Once several strain gauges deviate due to presence of a nearby defect or crack, the PCA should produce additional vector. Reverse calculation of the components affecting the PCA vectors can identify the suspected strain gauges.

Finally, the Isolated Forest machine learning algorithm for anomalies detection was employed. The isolated forest algorithm is based on decision trees, and is implemented in an unsupervised fashion with no pre-defined labels. It is assumed that anomalies are few and distinct among the database, and therefore can be identified using decision trees as those having the least probability to occur. In this study the applicability of the isolated forest to detect cracks in full scale fatigue test was demonstrated.

4.2 Remote load monitoring and airworthiness assessment of inflatable aerostat structure using fiber optic sensing technology (I. Kressel, IAI, G. Gur-Arieh, IAF)

Inflatable aerostat systems provide significant load carrying capabilities compared to other unmanned systems. The complexity of aerostat fabric structure imposes significant challenges for engineers in designing, analyzing, and testing. An important step in the development of an aerostat system, is monitoring the structure during its development. This must be accomplished by quantitative assessment of stress and strains developed in the fabric as a result of the induced aerodynamic loading, internal pressure and payload weight.

Common strain measurement systems for metallic parts cannot be used directly on such flexible fabrics. Indeed, the strains developed in the fabric based Inflatable Aerostat structures can be larger by orders of magnitude than the typical strains of standard metallic structures. Furthermore, the ability to measure strains while the aerostat system is high in the sky requires most electrical strain measurement instrumentation to be on board and transmit the data through a significant distance to the ground. Thus, there is an obvious advantage to the selected strain measurement technique where all instruments remain on ground while measuring the strains in chosen locations up in the sky. Finally, the ability to monitor strains in real-time, allowing to make go\no-go decisions during the testing period. All the aforementioned challenges necessitate an "atypical" strain measurement system.

Nowadays, optical fibers, bonded to the surfaces of structures or embedded within them, provide means to measure strain under both static and dynamic scenarios. Optical fiber sensing techniques include both discrete strain measurement technologies (e.g., using a number of Fiber Bragg Gratings (FBGs) at pre-chosen locations along the fiber) as well as distributed measurement of strain using Rayleigh-backscattering-based sensing that allows the monitoring of strains along several dozen meters of a standard single mode optical fiber, while keeping a spatial resolution of 5 mm, or even higher.

The use of optical fiber-based sensing technology for monitoring the aerostat fabric has several unique advantages. The optical fiber can sustain high strains exceeding 10,000 micro strains. Strain readings demonstrate linear behavior to the fiber elongation over the measurement range. Several sensors can be multiplexed on a single fiber, reducing the field application effort. They are flexible and can tolerate the ever-lasting bending of the aerostat fabric under operation. Optical fiber sensors of types used here are passive, they are immune to electrical interferences and do not generate any. A suitable interrogator is capable of reading them remotely (up to several kilometers) and to transform the optical signal into a standard digital format.

The first step in applying the sensing technology was to compare the performance of distributed fiber-optic strain sensor against a standard electrical strain gauge. This test, assisted by the aerostat manufacturer, was performed in the laboratory on a piece of the aerostat fabric. The test demonstrated the advantage of the optical fiber sensor over the electrical strain gauge, while the optical sensor kept measuring up to failure of the fabric, the electrical sensor peeled off

prematurely. Also, the readings of the optical sensor indicated that the stiffness of the electrical sensor induced inaccurate results. At the second stage of the concept development, the technology was applied during a development test conducted by the Original Equipment Manufacturer (OEM). Accurate measurements were recorded, demonstrating the ability of applying the fiber sensing technology onto complex large-scale testing. As a final step, a real-time optical sensor-based monitoring system was installed on an aerostat as an airworthiness evaluation tool. Optical fiber sensors (FBG type) were bonded to the aerostat inner surface at critical locations. The sensors were remotely read by an on-ground interrogator through optical fibers in the aerostat tether.

The implemented optical fiber-based sensing system has robustly and continuously collected strain data for already over one year. The effects of events such as payload loading/unloading, stresses under strong winds, etc., are clearly identified in the recorded strain map. To the best of our knowledge, this real time, optical fiber-based, aerostat monitoring system, applied as decision support tool on an operational aerostat to evaluate its mechanical integrity, is the first of its kind.

5. MISCELLANEOUS

5.1 Ti-6Al-4V Additive manufacturing measure of quality according to fatigue crack initiation vs. crack propagation (C. Matias, IAI)

Additive Manufacturing (AM) of metallic alloys was recognized by the aviation industry as a disruptive technology that can change the way aviation products are designed and fabricated. While the production of AM structural parts is proven to be cost effective, it usually requires multiple secondary processes such as machining, heat treatment, surface finish, and non-destructive inspections, which are costly, thus significantly affecting the insertion of AM products to serial productions. As a result, it appears that AM applications are mainly found as secondary structural items that does not participating in carrying flight loads (such as fairings, brackets, etc.). These items generally do not require high levels of quality control as required for primary structural items.

The objective of this study is to determine the requirements for non-destructive evaluation that will ensure sufficient strength, fatigue and crack growth characteristics. To this end, several AM specimens were fabricated, as shown in Figure 25, spanning various printing parameters and heat treatment procedures.

Figure 25: Fatigue test specimens and

The effect of three types of defects (voids/pores, lack of fusion, inclusions) on strength, fatigue and crack growth properties of the AM specimens was studied (typical defects were measured using Micro-CT before testing). While these defects have only negligible effect from crack growth point of view, an appreciable effect was observed in crack initiation testing (S-N curves). This observation is shown in Figure 26. In this figure, the effect of the heat treatment as well as HIP is also shown.

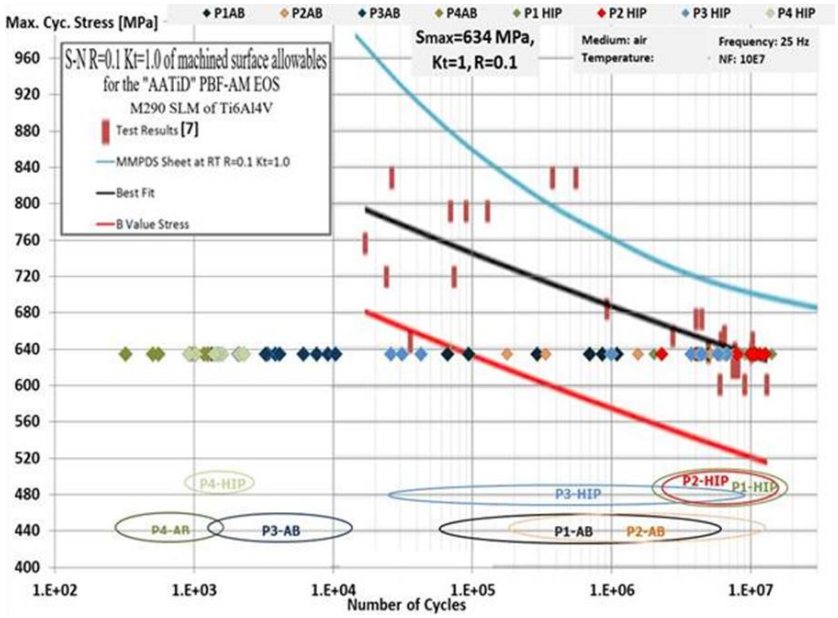

Figure 26: Effect of different printing parameters (and consequently different defects) and heat treatment on fatigue lives

The following conclusions were drawn:

- For generally good quality printing parameters, the HIP procedure was found to be effective to improve fatigue lives, as well as reducing the test results scatter.
- For poor printing parameters, the HIP procedure had an opposite effect on the fatigue lives, especially in terms of test scatter
- Minimal defect sizes that still provides sufficient fatigue lives were determined. The traditional usage of relative density as a measure of the fabrication quality was discussed, and it was shown that its reliability is questionable. It was shown that even for cases of very high relative density (> 99.999%), if the defects are in the vicinity of the free surface (as shown in Figure 27), short fatigue lives are reported. Consequently, new pass/fail criterion that includes the defect size and its proximity to the surface was proposed

The study is fully described in two conference papers [3, 4].

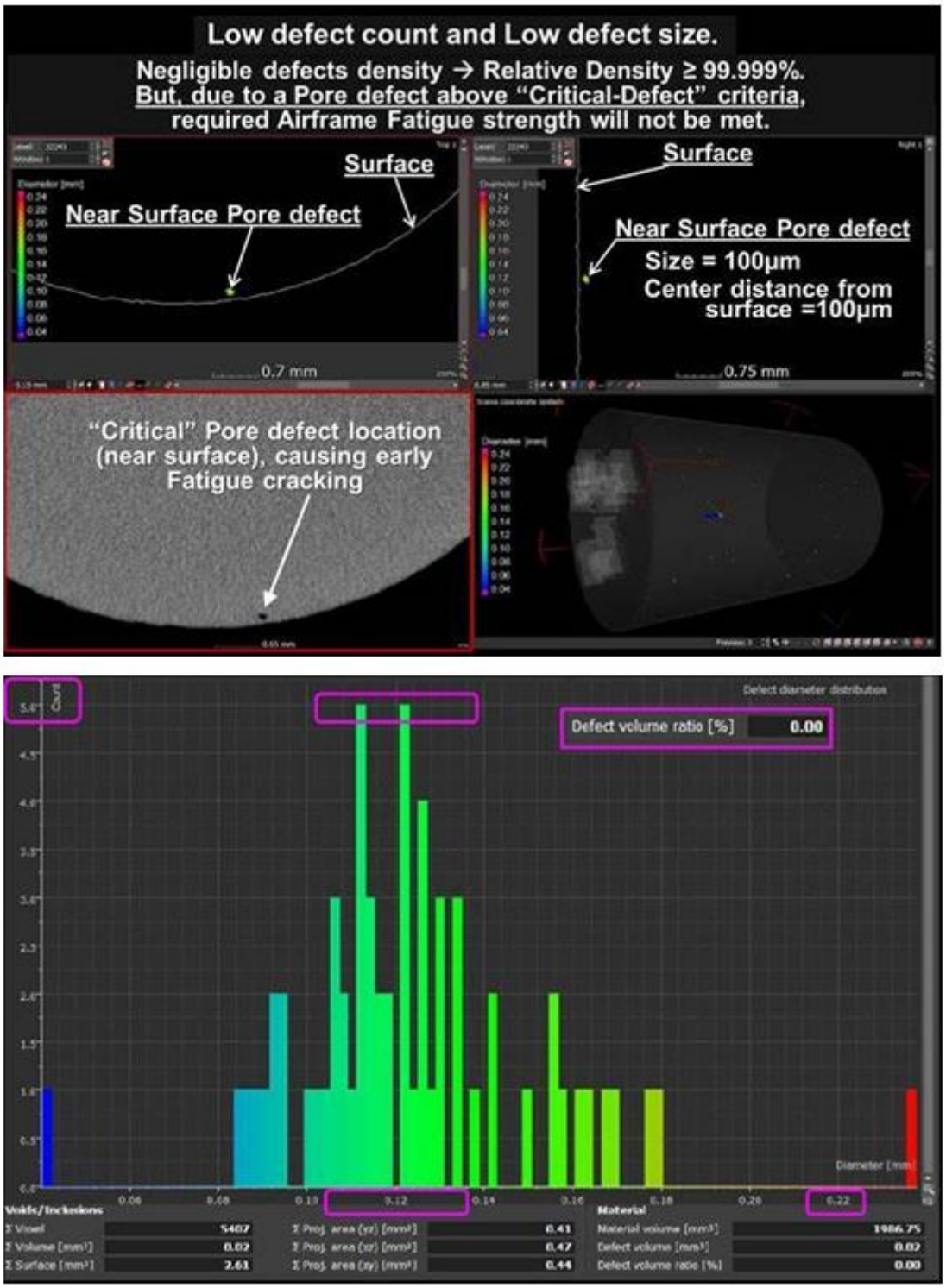

Figure 27: An example of specimen with small number of defects (relative density > 99.999%) but with short crack growth life. The early fatigue failure is contributed to the proximity of the defect to the surface

5.2 Predictions of high cycle fatigue life for additive manufacturing Ti-6Al-4V as a function of the internal microstructural defects using machine learning (M. Mega, Ariel University)

Additive Manufacturing (AM) techniques are able to fabricate parts with complex geometries and low buy-to-fly ratios for allowing lightweight structures by topological optimization implementation for the aerospace industry. However, due to defects created by the manufacturing process, these materials have unreliable fatigue performances. Thus, currently AM techniques are not being used to manufacture vital structural elements. The main objectives of this research are to train Deep Learning models to perform fractographic analysis, as well as identify the initiation sites of fatigue cracks and defects from SEM images of the fractured surface of the specimen.

Then, Machine Learning Algorithms (MLAs) will be used to establish a correlation between the characteristics of defects (e.g. size, distance from the surface, shape, etc.) and the fatigue life of a specimen. By identifying the characteristics of critical defects, a control system will be developed to detect such critical defects from nondestructive microcomputer tomography scans that were obtained prior to the fatigue testing. Additionally, in this research the defects causing failure in selective laser melting (SLM) Ti-6Al-4V fatigue specimens will be compared to those observed in electron beam melting (EBM) Ti-6Al-4V fatigue specimens.

In this study, 37 selective laser melting (SLM) Ti-6Al-4V fatigue specimens were manufactured using three different build parameters and either underwent stress relief at 800◦C or Hot Isostatic Pressing (HIP) treatments. Additionally, 15 electron beam melting (EBM) Ti-6Al-4V fatigue specimens were investigated. The fatigue life of each specimen was determined via tension-tension fatigue testing. After failure, each specimen surface was examined with a high-resolution scanning electron microscope (SEM). For each sample, three SEM images with the increased focus of the initiation site and increasing pixel sizes of 1.34, 0.38, and 0.15 µm, were obtained. Note that a 16-cell grid of the total specimen scan was used to obtained the 0.38 µm pixel size images. The chosen used cell is the one containing the initial failure site. In Figure 28, three SEM images of the same specimen with increased focus and pixel size, are presented. All images were scanned in a resolution of 4096×4096 pixels. Note that the cause of failure for the specimen presented in Figure 28 is a lack of fusion (LOF) defect. However, the cause for LOF, which may be a result of a pore or an inclusion, was not specified.

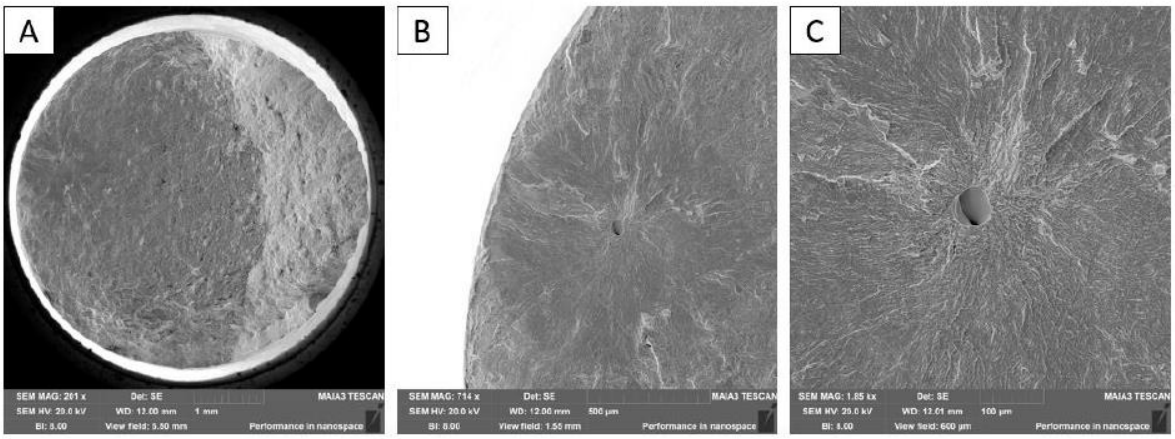

Figure 28: SEM images with different pixel size (A) the entire fractured surface with pixel size of 1.34 µm, (B) cell containing the initiation site with pixel size of 0.38 µm and (C) focused high resolution image of the initiation site with pixel size of 0.15 µm

7 REFERENCES

1. Freed Y., “Review of Aeronautical Fatigue Investigations in Israel, January 2019 – December 2020”, Minutes of the 37th ICAF Webinar, 2021.

2. Levi-Sasson A., Freed Y., "Failure Envelope for EA 9394 Paste Adhesive under Mixed Mode Stress Conditions for Composite Adhesive Joints", 61st Israel Annual conference on Aerospace Sciences, 2022, Tel Aviv, Israel.

3. Matias C. et al., "Effects of Additive Manufacturing inherent defects on the Fatigue behavior of Ti-6AL-4V: An experimental study", 61st Israel Annual conference on Aerospace Sciences, 2022, Tel Aviv, Israel.

4. Matias C. et al., "Ti-6AL-4V Additive Manufacturing Measure of Quality According to Fatigue Crack Initiation vs. Crack Propagation", 33rd Congress of the International Council of the Aeronautical Sciences, 2022, Stockhom, Sweden.

5. Sause, M. G., Schmitt, S., & Kalafat, S., Failure load prediction for fiber-reinforced composites based on acoustic emission. Composites Science and Technology, 164, 24-33, 2018.

6. Patel, D. K., Parthasarathy, T., & Przybyla, Predicting the effects of microstructure on matrix crack initiation in fiber reinforced ceramic matrix composites via machine learning. Composite Structures, 236, 111702, 2020.

7. Zobeiry, N., Reiner, J., & Vaziri, R., Theory-guided machine learning for damage characterization of composites. Composite Structures, 246, 112407, 2020.

8. Reiner, J., Vaziri, R., & Zobeiry, N., Machine learning assisted characterisation and simulation of compressive damage in composite laminates. Composite Structures, 273, 114290, 2021.

9. Freed Y., Zobeiry N. and Salviato M., Development of aviation industry-oriented methodology for failure predictions of brittle bonded joints using probabilistic machine learning, Composite Structures, 297: 115979, 2022.

10. Freed Y., Salviato M, and Zobeiry N., Implementation of a probabilistic machine learning strategy for failure predictions of adhesively bonded joints using cohesive zone modeling, International Journal of Adhesion and Adhesives, 118: 103226, 2022.

11. Freed Y., Implementation of machine learning strategies for determination of finite width correction factors for orthotropic plates containing central hole, Journal of Composite Materials, 56(28), p. 4221-4230, 2022

12. Freed Y., Koren M. and Dorfman B., Aircraft loads assessment and its effect on aircraft structure = machine learning approach, 62nd Israel Annual Conference on Aerospace Sciences, 2023, Tel Aviv, Israel

13. Aviation Investigation Report A05F0047, Transportation Safety Board of Canada, 2005 (https://www.tsb.gc.ca/eng/rapports-reports/aviation/2005/a05f0047/a05f0047.html)

14. FAA Press Release, FAA Proposes $2.4 Million Civil Penalty Against Cessna Aircraft, September 22, 2011

15. da Silva, LFM., Öchsner, A. and Adams, RD. eds., 2011. Handbook of adhesion technology (Vol. 1, p. 1543). Heidelberg: Springer.

16. Baker A, Gunnion AJ, Wang J, Chang P. Advances in the proof test for certification of bonded repairs–Increasing the Technology Readiness Level. International Journal of Adhesion and Adhesives. 2016 Jan 1;64:128-41.

17. Laser bond line inspection becomes reality, CompositeWorld, 2.8.2022. https://www.compositesworld.com/articles/laser-bondline-inspection-becomes-reality.

18. EASA CM-S-005. Bonded repair size limits in accordance with CS-23, CS-25, CS-27, CS-29 and AMC 20-29.

19. EASA CM-S-010. Composite materials - the safe design and use of monocoque sandwich structures in principal structural element applications.

20. Ashforth C, Ilcewicz L. Certification of bonded aircraft structure and repairs. NATO STO-MP-AVT-266, 2018. https://doi. org/10.14339/STO-MP-AVT-266-06-PDF; 2018.

21. NATO - STANAG 4671, Unmanned Aircraft Systems Airworthiness Requirements (USAR)

22. Camanho, P. P., Erçin, G. H., Catalanotti, G., Mahdi, S., & Linde, P., A finite fracture mechanics model for the prediction of the open-hole strength of composite laminates. Composites Part A: Applied Science and Manufacturing, 43(8), 1219-1225, 2012.

23. Freed Y., G280 Executive Jet – Full Scale Fatigue Testing, 52nd Israel Annual Conference on Aerospace Sciences, 2012, Tel Aviv, Israel.

24. Buimovich Y., Freed Y., Noivirt G. and Matias C., A summary of the G280 executive jet full scale fatigue test, 56th Israel Annual conference on Aerospace Sciences, 2016, Tel Aviv, Israel

25. Shoham S., Dorfman B., Kressel I. and Tur. M., Structural Characteristics Pattern Recognition Algorithm for Health and Usage Monitoring, 58th Israel Annual Conference on Aerospace Sciences, 2018, Tel Aviv, Israel.

26. Schapira Y. and Yosibash Z., Asymptotic solution of the elasticity equations in the vicinity of an elliptical crack front, Engineering Fracture Mechanics, 223, article 106774, (2020)

27. Yosibash Z. and Schapira Y., Edge stress intensity functions along elliptic and part-elliptic 3D cracks, Engineering Fracture Mechanics, 245, article 107477, (2021)

28. Schapira Y., Omer N. and Yosibash Z., The T-stress along a 3-D straight crack, Engineering Fracture Mechanics, 202, pp. 214-241, (2018)

29. Yosibash Z. , V. Mendelovich, I. Gilad and A. Bussiba, Can the finite fracture mechanics coupled criterion be applied to V-notch tips of a quasi-brittle steel alloy?, Engineering Fracture Mechanics, 269, article 108513, (2022)

30. Hu T., Dolbow J.E. and Yosibash Z., Towards validation of crack nucleation criteria from V-notches in quasi-brittle metallic alloys: Energetics or strength?, Methods in Applied Mechanics and Engineering, 402, article 115419, (2022)

31. Bussiba, A., Gilad, I., Lugassi, S., David, S., Bortman, J. and Yosibash Z. , Mechanical Response and Fracture of Pultruded Carbon Fiber/Epoxy in Various Modes of Loading, Crystals , 12, article 850, (2022)

32. Perl M, Kamal SM, Mulera S. The Use of an Equivalent Temperature Field to Emulate an Induced Residual Stress Field in a Rotating Disk Due to Full or Partial Rotational Autofrettage. Journal of Pressure Vessel Technology. 2022 Dec 1;144(6):061301.

33. Perl M, Saley T. Internal Versus External Cracking—Their Impact on the Fatigue Life of Modern Smoothbore Autofrettaged Tank Gun Barrels. Journal of Pressure Vessel Technology. 2021 Apr 1;143(2).

34. Levy C, Perl M, Ma Q. The Effect of a Three-Dimensional Quarter-Circle Corner Crack on the Stress Intensity Factors of a Nonaligned Semi-Elliptical Surface Crack in an Semi-Infinite Solid Under Uniaxial Tension. Journal of Pressure Vessel Technology. 2021 Jun 1;143(3).

35. Ma Q, Perl M, Levy C, The interplay between an edge crack and a parallel internal crack in an infinite sheet under in-plane bending, Journal of Research in Mechanical Engineering 8(2), p. 23-36, 2022.

36. Katzeff S., An Investigation Into Curved Beam Flange Efficiency in Thin-Walled Structure, 62nd Israel Annual Conference on Aerospace Sciences, 2023, Tel Aviv, Israel